THE JOURNAL OF PHYSICAL CHEMISTRY B
A JOURNAL OF THE AMERICAN CHEMICAL SOCIETY

pubs.acs.org/JPCB

Article

Structural Rearrangement of the AT1 Receptor Modulated by Membrane Thickness and Tension

Published as part of The Journal of Physical Chemistry B special issue "Membrane Protein Simulations".

Bharat Poudel and Juan M. Vanegas*

Cite This: *J. Phys. Chem. B* 2024, 128, 9470–9481

Read Online

ACCESS | Metrics & More | Article Recommendations | Supporting Information

ABSTRACT: Membrane-embedded mechanosensitive (MS) proteins, including ion channels and G-protein coupled receptors (GPCRs), are essential for the transduction of external mechanical stimuli into biological signals. The angiotensin II type 1 (AT1) receptor plays many important roles in cardiovascular regulation and is associated with diseases such as hypertension and congestive heart failure. The membrane-mediated activation of the AT1 receptor is not well understood, despite this being one of the most widely studied GPCRs within the context of biased agonism. Here, we use extensive molecular dynamics (MD) simulations to characterize the effect of the local membrane environment on the activation of the AT1 receptor. We show that membrane thickness plays an important role in the stability of active and inactive states of the receptor, as well as the dynamic interchange between states. Furthermore, our simulation results show that membrane tension is effective in driving large-scale structural changes in the inactive state such as the outward movement of transmembrane helix 6 to stabilize intermediate active-like conformations. We conclude by comparing our simulation observations with AlphaFold 2 predictions, as a proxy to experimental structures, to provide a framework for how membrane mediated stimuli can facilitate activation of the AT1 receptor through the β-arrestin signaling pathway.

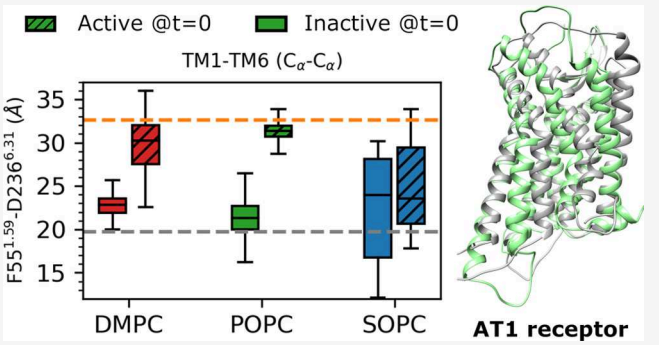

INTRODUCTION

Mechanical signal transduction, the process of converting external physical stimuli into biochemical signals, plays a fundamental role in many biological processes.[1−3] This conversion process is often mediated by membrane-embedded mechanosensitive (MS) proteins, which respond to deformations in the membrane caused by stimuli such as tension or shear through what is known as the "force-from-lipid" principle.[2] In bacteria, MS channels such as MscL and MscS are part of the machinery that regulates turgor pressure and prevents cell lysis during hypo-osmotic shock.[1,4,5] In higher organisms, MS proteins such as the two-pore domain potassium (K2P)[6−8] and the Piezo1/2[9−11] ion channels are essential for cardiovascular control and development, touch sensing, and proprioception among many other biological functions.[3] However, ion channels are not the only proteins whose function is modulated by membrane-mediated forces as many G-protein coupled receptors (GPCRs) have been shown to initiate unique signaling pathways in response to mechanical stimuli in the absence of a chemical agonist.[12] Some of these mechanically activated GPCRs include the angiotensin II (AngII) type 1 (AT1) receptor,[13−16] the sphingosine-1-phosphate receptor (S1PR1),[17] the muscarinic acetylcholine receptor M3 (M3R),[18] the formyl peptide receptor (FPR),[19] the bradykinin receptor B2 (BDKRB2),[20] and the dopamine receptor D_5R[21] among others.

The AT1 receptor is one of the most widely studied GPCRs in the context of biased agonism as it plays a pivotal role in a diverse range of physiological processes in the human body whose function regulates hypertension and congestive heart failure.[22−24] Agonist-induced signaling initiated by the AT1 receptor occurs through the $G\alpha_q$ or β-arrestin 2 (β-arr2) pathways where balanced agonists such as the vasoconstricting peptide AngII induce both, while biased agonists such as the peptides TRV055 and TRV023 favor only the $G\alpha_q$ or β-arr2 pathway, respectively.[25] Stretch-induced activation of the AT1 receptor in the absence of an agonist has been shown to activate the β-arr2 signaling pathway.[14,15,25] An early study suggested that this mechanical activation occurred through direct interaction with β-arr2,[26] but more recent evidence

Received: May 20, 2024
Revised: September 9, 2024
Accepted: September 10, 2024
Published: September 19, 2024

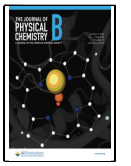

https://doi.org/10.1021/acs.jpcb.4c03325
J. Phys. Chem. B 2024, 128, 9470−9481

suggests that $G\alpha_i$ is necessary for the recruitment of β-arr2 under physical stimulation.[15,27]

GPCRs, along with many other membrane proteins, are highly sensitive to the chemical (e.g., different headgroups such as phosphoethanolamine or phosphocholine) and physical (e.g., thickness and curvature) properties of their local membrane environment.[28−35] Oligomerization of GPCRs is strongly mediated by lipid interactions,[30,32] and changes in membrane composition have been associated with age-related health disorders through modulation of GPCR signaling pathways.[31] It has been recently shown that even shallow changes in membrane curvature are sufficient to spatiotemporally control the organization of GPCRs within the plasma membrane.[36] Changes in the hydrophobic thickness of the plasma membrane, causing a mismatch with the embedded proteins, play an important role in the modulation of protein function.[28,33] Biophysical studies on rhodopsin[37−39] and ghrelin,[40] the growth hormone secretagogue (GHS) receptor, have shown that these GPCRs are highly sensitive to bilayer thickness and function optimally at particular chain lengths, which may be receptor specific.

Understanding the role of mechanical stimuli such as osmotic stretch on the function of membrane proteins is very challenging because the effects of lateral pulling forces are not easily decoupled from other physical changes such as the decreased bilayer thickness due to area expansion. This is further complicated *in vivo* as biological membranes have broad lipid compositions and have large asymmetries between leaflets,[41] both of which can affect the overall mechanical response.[42,43] Within the context of the MS channel MscL, we have shown through local stress calculations[44,45] in molecular dynamics (MD) simulations that the distribution of forces on the surface of the channel under membrane tension is largely asymmetric with stress "hot-spots" where forces are concentrated during gating.[46] Moreover, MscL's flexible α-helical architecture allows the channel to undergo a "silent" area expansion,[47] serving as a mechanical strain buffer, during the initial stages of gating before the inner pore becomes hydrated and the helices tilt and expand to create the large 25−30 Å pore.[47,48] In the AT1 receptor, we have shown that various membrane conditions and stimuli, including tension, can stabilize active-like conformations in the absence of any ligand through extensive MD simulations (up to 20 μs) using the Anton 2 supercomputer in addition to well-tempered metadynamics free energy calculations.[49] However, it remains unclear whether comparable structural changes in the inactivated apo-AT1 receptor can be induced through membrane-mediated interactions.

Here, we present a comprehensive MD simulation study that systematically examines how changes in membrane thickness, by varying the acyl chain length as well as membrane tension, modulate the structural features of the AT1 receptor when simulated in both active and inactive starting configurations. We leverage access to the Anton 2 supercomputer to run extensive MD simulations, ranging from 5 to 20 μs with multiple replicas, under various membrane conditions for a total simulation time >175 μs. We show that long simulation time scales are essential to capture the relatively slow dynamics of the receptor, where many transitions happen in the range of 0.5−1 μs and intermediate states may persist over multiple microseconds. Our results also show that exploration of different conformational states of the AT1 receptor through MD simulations may be strongly affected by the initial structure depending on the membrane conditions.

METHODS

System Setup and Initial Equilibration. Initial molecular dynamics (MD) simulations were run with the GROMACS simulation package[50] (version 2021.2) using the CHARMM36m force-field.[51−55] This force-field includes optimized parameters for lipids, proteins, water, and ions. Water was simulated with the modified CHARMM TIP3P model with additional van der Waals parameters on the H atoms. The initial configuration for the active state of the AT1 receptor was taken from Wingler et al.[56] (PDBID: 6DO1). Protonated states of residues $D74^{2.50}$ and $D125^{3.49}$ were employed to preserve local interactions within the low hydration environment.[57] Superscripts next to residue numbers follow the Ballesteros−Weinstein[58] numbering scheme, which is based on the presence of highly conserved residues in each of the seven transmembrane (TM) helices. The loop connecting TM5 and TM6, which was not resolved in the original structure, was modeled using the MODELLER v9.12 package.[59] Due to the inclusion of this additional loop, the AT1 receptor sequence used deviates by five residues from TM6 onward in comparison to other conserved G-protein-coupled receptor (GPCR) residues. In all simulations, the AT1 receptor was embedded within equilibrated membrane patches consisting of 100 lipids (50 in each leaflet). Lipids included dimyristoyl-*sn*-glycero-3-phosphocholine (DMPC), 1-palmitoyl-2-oleoyl-glycero-3-phosphocholine (POPC), and 1-stearoyl-2-oleoyl-*sn*-glycero-3-phosphocholine (SOPC). To prevent interactions with periodic images, a substantial water layer (>1.2 nm) was introduced including a 0.15 KCl ionic concentration. Following 1000 steps of energy minimization, all membrane−protein systems underwent an initial 25 ns equilibration simulation with protein-only position restraints (k = 1000 kJ/mol/nm^2) under constant temperature (37 °C) and pressure (1 atm) using a Berendsen thermostat and a semi-isotropic Berendsen barostat.

Production Simulations on Anton 2. After the initial membrane equilibration with the protein under position restraints, production simulations were completed on the Anton 2 supercomputer.[60] The equations of motion were integrated using the multigrator method with a 2.5 fs time step.[61] Short-range forces were evaluated at every time step, and long-range electrostatics were calculated every three time steps using the Gaussian split Ewald method.[62] Van der Waals interactions were computed by using a 1.2 nm cutoff. System pressure was kept constant at 1 atm using a semi-isotropic Martyna−Tobias−Klein (MTK)[63] barostat with a coupling frequency of 480 steps. Temperature was kept constant with a Nosé−Hoover thermostat at 37 °C and a coupling frequency of 24 steps. Positions were saved in 240 ps time intervals. For most systems, two replicas were simulated starting from the same initial structure but with different initial velocities drawn from a Maxwell distribution. All systems were simulated for 5 μs, and some were extended to 10 and 20 μs.

For simulations under membrane tension, the γ_{zz} element of the tension_ref array in the Anton 2 ARK recipe is changed from the default value of 0 to values ranging from 1 to 20 mN/m. For example, for a membrane tension of 15 mN/m, the tension_ref array is set to [0, 0, 0, 0, 0, 0, 0, 0, −3000], where the units are in bar·Å. A factor of 2 is included to take into account the two interfaces of the lipid bilayer. For simulations

https://doi.org/10.1021/acs.jpcb.4c03325
J. Phys. Chem. B 2024, 128, 9470−9481

starting from the inactive state, we extracted a simulation frame at t = 5 μs from a tensionless SOPC simulation taken from our previous work[49] where the receptor spontaneously returns to the inactive state and the TM1−TM6 distance had reached a value of 21.5 Å. Similarly, for simulations starting from intermediate configurations, we took frames from the same simulation trajectory at 0.3 and 1 μs, where the values of the TM1−TM6 distance were approximately 28 and 25 Å, respectively.

Data Analysis. For characterization of the structural differences between active and inactive states of the AT1 receptor, we measured the transmembrane distances based on previous electron paramagnetic resonance studies of activation/inactivation.[64] The Cα atoms of residues F55$^{1.59}$, R126$^{3.50}$, and D236$^{6.31}$ were used to compute the TM1−TM6 and TM3−TM6 distances. Three other residue pairs were used to compute distances between their centers of mass for L78$^{2.54}$−Y292$^{7.43}$ and S115$^{3.39}$−N295$^{7.46}$, and between the hydroxyl oxygens for Y215$^{5.58}$−Y302$^{7.53}$. A moving average (i.e., a rolling mean) with a window of 5 data points was applied to all plots showing the time evolution of the various distances explained above.

The average thickness of the lipid membrane was determined by analyzing the time-averaged phosphorus atom density along the z-axis in both leaflets and measuring the distance between peak points. The laterally resolved cytoplasmic or periplasmic leaflet thickness was obtained from the time-averaged positions of the phosphorus atoms relative to the bilayer midplane. The positions of the TM helices near the phosphate region, shown as circles in the leaflet thickness plots, were obtained by computing the time-averaged center of mass of the first or last three residues of each helix, depending on its orientation relative to the membrane. All visual representations were generated using the Matplotlib library.[65] Molecular models of the AT1 receptor were constructed using UCSF Chimera and ChimeraX.[66,67]

AlphaFold 2 Predictions. AlphaFold 2[68] structural predictions were obtained using a local ColabFold[69] installation (version 1.5.5) which queries the MMseqs2 server for the multiple sequence alignment.[70,71] Protein sequences were obtained from the Uniprot database[72] using the following accession numbers: P30556 for the human AT1 receptor, P32121 for human β-arr2, P63096 for human Gα_{i1}, P04899 for human Gα_{i2}, and P50148 for human Gα_{q}. Five independent predictions were run to obtain the structure of the monomeric apo-AT1 receptor, as well as the multimeric AT1R:Gα_{i1}, AT1R:Gα_{i2}, AT1R:Gα_{q}, and AT1R:β-arr2 complexes. ColabFold produced 5 structural predictions, and the top ranked model was used for visualization. The AlphaFold 2 predictions were colored based on the predicted local distance difference test (pLDDT) score, which is a per-residue measure of local confidence. pLDDT scores are scaled from 0 to 100, and they estimate how well a prediction would agree with an experimental structure.

RESULTS AND DISCUSSION

Stability of Inactive and Active-like States. As crystallographic structures of the AT1 receptor are determined either in agonist-bound active (e.g., PDBID: 6OS0) or antagonist-bound inactive (e.g., PDBID: 4YAY) conformations (see Figure 1), we test the effect of simulating the apo receptor starting from both types of conformations in pure phosphatidylcholine (PC) bilayers featuring distinct acyl chain lengths

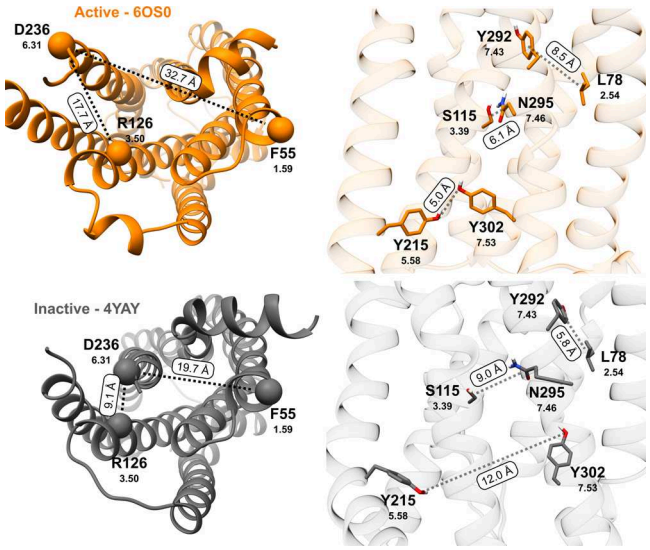

Figure 1. Ribbon illustrations of the active (orange) and inactive (gray) configurations of the AT1 receptor showing residues selected to quantitatively describe activation and inactivation. Left panels show the cytoplasmic side of the receptor highlighting the Cα atoms of residues F55$^{1.59}$, R126$^{3.50}$, and D236$^{6.31}$ used to compute the TM1−TM6 and TM3−TM6 distances. Right panels show three residue pairs used to compute distances between their centers of mass for L78$^{2.54}$−Y292$^{7.43}$ and S115$^{3.39}$−N295$^{7.46}$ and between the hydroxyl oxygens for Y215$^{5.58}$−Y302$^{7.53}$. Superscripts follow the Ballesteros−Weinstein[58] numbering scheme.

including DMPC (di-C14:0), POPC (C16:0,C18:1), and SOPC (C18:0,C18:1) at a physiological temperature of 37 °C. Following energy minimization, each system underwent a 25 ns membrane pre-equilibration period where position restraints were imposed on the protein to prevent large conformational changes in the receptor while the surrounding lipids undergo initial arrangements. This equilibration phase was followed by two independent 5 μs unrestrained simulation runs on the Anton 2 supercomputer, each initiated with different initial velocities for all atoms (see Methods).

Beginning with the AT1 receptor simulated from the active state, we characterized large-scale motions of the TM helices through distances between F55$^{1.59}$ and D236$^{6.31}$ (TM1−TM6) as well as R126$^{3.50}$ and D236$^{6.31}$ (TM3−TM6) as shown in Figure 2 and Figure S1. Superscripts follow the Ballesteros−Weinstein[58] numbering scheme, which is based on the presence of highly conserved residues in each of the seven TM helices. The distances between TM6 and TM1/TM3 capture the outward/inward motion of TM6 which is essential for binding of effector partners such as G-proteins and β-arrestins. Moreover, TM3 contains residue R126$^{3.50}$ that is a part of the highly conserved DRY motif. Analysis of the time traces in the two replicas reveals significant fluctuations in these two distances for the AT1 receptor in the SOPC membrane (longest chain length), which switches between various active-like, intermediate, and inactive values over the 5 μs period (Figure 2a,b and Figure S1). The TM1−TM6 distance returns to the fully inactive value (∼20 Å) in the first replica of SOPC, while for the second replica it explores an intermediate value near 24 Å for over 1 μs before returning to active-like values of ∼29−32 Å in the later stages of the 5 μs simulation (Figure 2a). While only one replica is shown in Figure 2 for clarity, we include box and whisker plots analyzing

https://doi.org/10.1021/acs.jpcb.4c03325
J. Phys. Chem. B 2024, 128, 9470−9481

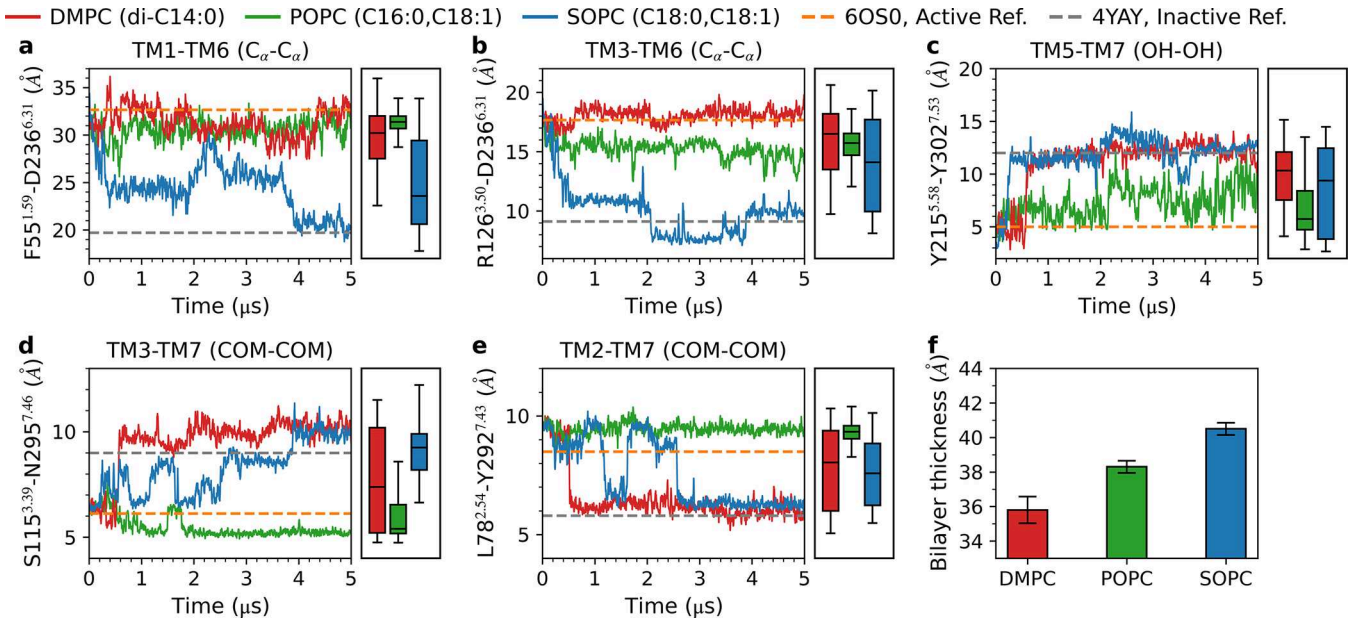

Figure 2. Time evolution of apo-AT1 receptor simulations starting from an active configuration embedded in PC membranes with varying chain lengths. Large-scale conformational changes describing the inward/outward movement of TM6 are depicted by the TM1−TM6 (a) and TM3−TM6 (b) distances, while reorientation of local microswitches are described by the Y215−Y302 (NPxxY motif) (c), S115−N295 (d), and L78−Y292 (e) distances. Rectangular boxes on the right of each panel show box and whisker plots including median, quartiles, and extrema of the combined data from the two replicas of each system over the last 500 ns. Dashed gray and orange lines show values from crystal structures of the inactive receptor bound to a selective antagonist (4YAY) and active receptor bound to AngII (6OS0), respectively. (f) Average bilayer thickness of the three PC membranes computed from the peak-to-peak distance of the bilayer mass density over the last 500 ns of the two replicas. Error bars show the standard deviation from the mean. An active-like configuration is most stable in the medium length POPC membrane.

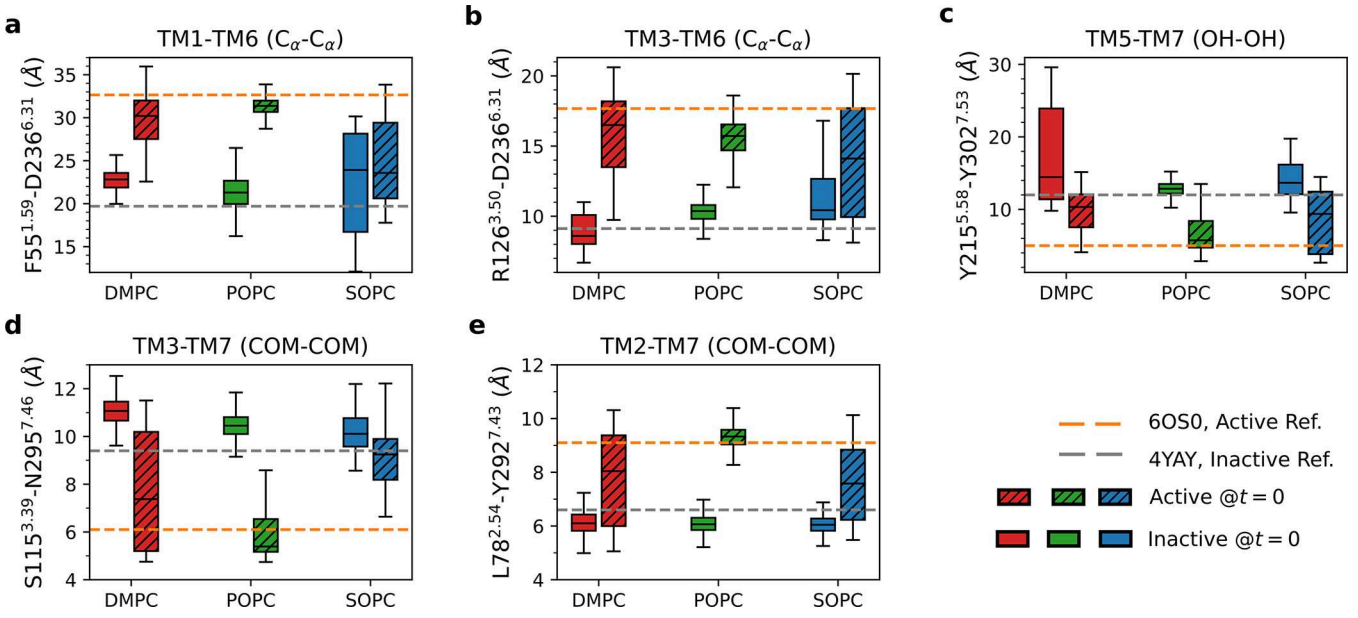

Figure 3. Stability of active-like and inactive states of the apo-AT1 receptor in PC membranes with varying chain lengths. For each membrane, the receptor is simulated starting from an active or inactive configuration and simulated for 5 μs, followed by analysis over the last 500 ns of the trajectory. Large-scale conformational changes describing the inward/outward movement of TM6 are depicted by the TM1−TM6 (a) and TM3−TM6 (b) distances, while reorientation of local microswitches are described by the Y215−Y302 (NPxxY motif) (c), S115−N295 (d), and L78−Y292 (e) distances using box and whisker plots (including median, quartiles, and extrema of the combined data from the two replicas of each system). Dashed gray and orange lines show values from crystal structures of the inactive receptor bound to a selective antagonist (4YAY) and active receptor bound to AngII (6OS0), respectively. Exploration of active- and inactive-like states is determined by both the acyl chain length as well as the initial simulation configuration.

the last 500 ns of the two replicas. The receptor in DMPC (the shortest chain length) shows greater stability near active-like values for TM1−TM6 and TM3−TM6, although it does explore intermediate values as seen in the second replica (Figure S1). In contrast to SOPC, medium chain length POPC appears to be consistently stable near the active values for both

https://doi.org/10.1021/acs.jpcb.4c03325
J. Phys. Chem. B 2024, 128, 9470−9481

of the TM distances. Beyond the movement of the TM helices, we also characterized the local reorientation of three specific microswitches. Two of these microswitches interact via H-bonding in the active state: The highly conserved Y302$^{7.53}$ in TM7 (part of the NPxxY motif) with Y215$^{5.58}$ in TM5 and S115$^{3.39}$ in TM3 with N295$^{7.46}$ in TM7. The NPxxY motif is a highly conserved region among class A GPCRs,[73] and comparison of active and inactive structures in the β_2-adrenergic-receptor have shown the importance of H-bonding between Y7.53 and Y5.58 to stabilize TM5 during Gα_i binding.[74] Lastly, Y292$^{7.43}$ in TM7 lines the receptor's binding pocket in the inactive state and has been identified as an important residue that modulates the effect of biased agonists.[56] Rearrangement of Y7.43 has been identified as an important regulator in the activation of the chemokine receptor CCR1.[75] We characterized the motion of Y292$^{7.43}$ through its distance to nearby F78$^{2.54}$. The values for the distances of these three microswitches appear to be most stable near the active state in the POPC membrane as seen in both replicas (Figure 2c−e and Figure S1). In the case of DMPC and SOPC, a clear pattern of stabilization for the microswitches is not as apparent as the distances either remain steady near the active values or quickly transition to inactive ones depending on the replica.

We now proceed to compare with simulations starting from the inactive state, with time traces shown in Figure S2 and Figure S3 and box and whisker plots for the last 500 ns shown in Figure 3. When simulated from the inactive configuration, the TM1−TM6 distances for all three membranes show fluctuations between inactive and intermediate (∼24 Å) values and in some cases reaching active-like (∼29 Å) values (Figure S2). However, the combined results from both replicas shown in Figure 3a indicate that the motion of TM6 is limited in the DMPC and POPC membranes with TM1−TM6 distances remaining close to the inactive values, while in SOPC this distance explores a larger range of motion. A similar pattern is observed for the TM3−TM6 distance where the values in the DMPC and POPC membranes hover around the inactive state and are more likely to fluctuate upward in SOPC (Figure 3b, Figure S2b, and Figure S3b). The distances in the microswitches are largely maintained near the initial inactive state values across all replicas (see Figure 3c−e and Figures S2 and S3). In the case of the second replica of the DMPC membrane (Figure S3c), the Y302$^{7.53}$−Y215$^{5.58}$ distance appears to increase beyond the value observed in the inactive state. This is caused by an increase in the tilt of TM5 to reduce the hydrophobic mismatch around this helix, which moves the cytoplasmic side of TM5 away from TM7. Together, our results suggest that the dynamics of both large-scale TM movements and changes in the microswitches are influenced by both the initial configuration and the thickness of the PC membranes. In the intermediate chain POPC, the AT1 receptor shows reduced conformational fluctuations and its structure remains close to the initial configuration, either active or inactive, as shown in Figure 4a. In contrast to this, the AT1 receptor in the SOPC membranes is more dynamic regardless of the initial simulation setup, allowing the protein to explore a broader range of conformations, which enables the receptor to transition from the active to inactive state as shown in Figure 4b.

To further examine the role of acyl chain length in the stability of the inactive and active-like states of the apo-AT1 receptor, we characterized the membrane thickness in the

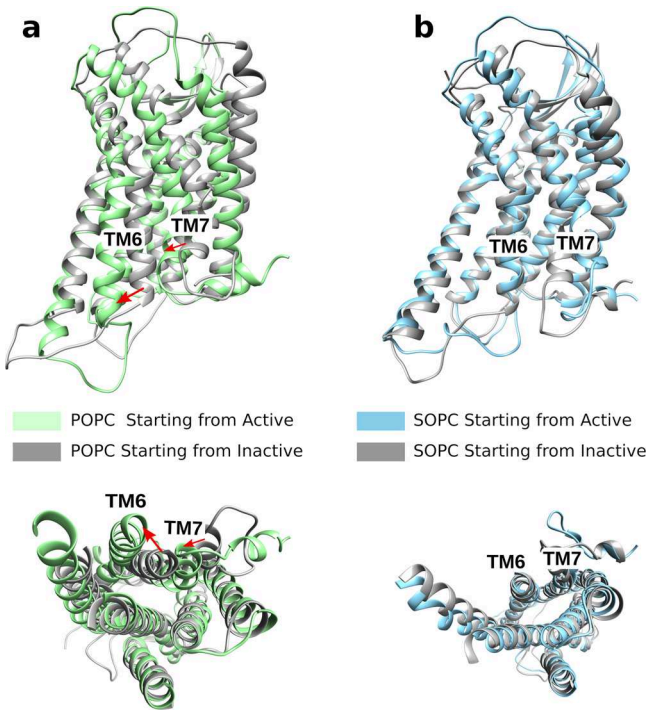

Figure 4. Structural comparison between simulations of the AT1 receptor starting from active and inactive configurations in POPC (A) and SOPC (B) membranes. Snapshots taken from the end of 5 μs simulations analyzed in Figure 3 showing side views (top panels) and cytoplasmic views (bottom panels). In POPC, the receptor remains in a similar configuration to the initial state (active or inactive). However, the receptor often explores intermediate and inactive states in the SOPC membrane regardless of the starting initial configuration.

vicinity of the protein. More specifically, Figure 5 shows the thickness of the cytoplasmic leaflet as computed from the time-averaged position of the phosphorus atoms relative to the bilayer midplane over the last 1 μs of the first set of replicas. Data for the second set of replicas is shown in Figure S4. When simulated starting from the active state, the isocontour maps show that in the thinner DMPC and POPC membranes, where the AT1 receptor remains stable in an active-like state, the cytoplasmic leaflet thickness near TM6 is in the range of 18−22 Å (Figure 5a,b). However, in the SOPC membrane where the receptor transitions to an inactive conformation, the cytoplasmic leaflet thickness near TM6 has a higher value in the range of 24−26 Å (Figure 5c). A similar pattern is observed in the inactive DMPC simulation (Figure 5d) as well as in the inactive POPC (Figure 5e) and SOPC (Figure 5f) simulations. It is surprising to observe such increase in the cytoplasmic leaflet thickness near TM6 in the DMPC system given that the average leaflet thickness is ∼18 Å. Panels a and b in Figure 5 clearly show the large distance between TM1 and TM6 on the cytoplasmic side in the active state, while in the inactive configurations (Figure 5c−f) TM6 moves inward toward TM1 and TM7 moves slightly outward. The TM helices do not undergo large displacements relative to each other on the periplasmic side of the membrane and therefore the leaflet thickness analysis does not reveal any obvious patterns between inactive and active-like states (Figure S5) except that the thickness near TM6 tends to be higher than in other regions for all systems.

One can interpret some of the observed patterns of stability of inactive and active-like states of the AT1 receptor from the

https://doi.org/10.1021/acs.jpcb.4c03325
J. Phys. Chem. B 2024, 128, 9470−9481

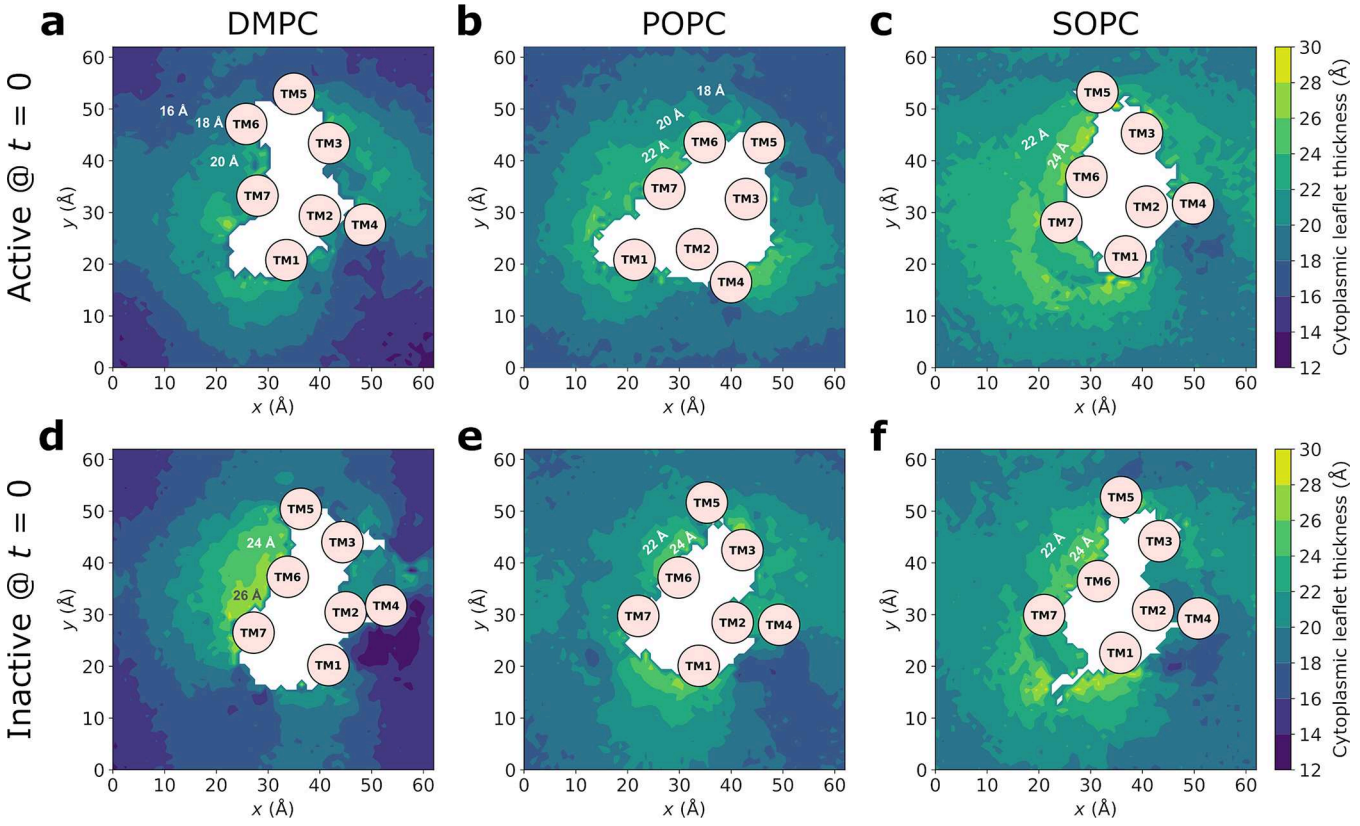

Figure 5. Cytoplasmic leaflet thickness in the vicinity of the AT1 receptor in DMPC (left), POPC (middle), and SOPC (right) membranes. Top row (a–c) shows isocontour maps for simulations starting from the active state, while bottom row (d–f) shows data for simulations of the AT1 receptor starting from the inactive state. Note that the initially active AT1 receptor transitions to an inactive state in the SOPC membrane (c). Leaflet thickness measured from the time-averaged position, over the period from 4 to 5 μs of replica 1, of the phosphorus atoms relative to the bilayer midplane. Location of the TM helices near the headgroup region shown with filled circles based on the center of mass of the four residues closest to the phosphate groups. The cytoplasmic leaflet thickness near TM6 is lower in the active-like states (a, b) compared to the inactive configurations (c–f).

perspective of the hydrophobic mismatch of the TM helices. TM6 has an approximate length of 47–48 Å, which means that it extends beyond the thickness of even the longest chain SOPC membrane. This is apparent in all the plots shown in Figure 5 where the leaflet thickness is always higher near the protein. As such, the hydrophobic regions of TM6 are kept from being exposed to the solvent through a combination of membrane deformation and tilting of the helix. In the thickest SOPC membrane, the outward/inward motion of TM6 is more likely to occur because the helix may only need to be minimally exposed to the solvent and/or the membrane deformed to transition between inactive and active-like states. On the other hand, the larger hydrophobic mismatch in the DMPC or POPC membranes creates a higher barrier for TM6 to transition between states, which results in the receptor being trapped in either of the two starting configurations. In addition to thickness, it is possible that the receptor may have different specific interactions with the saturated and unsaturated chains of the lipids used. To probe this, we analyzed the number of acyl chains (sn1 or sn2 separately) that are in contact with AT1 receptor (within 5 Å) as shown in Figure S6. This analysis does not show significant differences in the number of acyl chains that contact the protein when comparing different lipids, which indicates that there is no apparent interaction preference.

Tension-Mediated Activation of the AT1 Receptor. In our previous study (Poudel et al.[49]), we showed that moderate tensions in the range of 10–15 mN/m were more effective in stabilizing active-like states in the AT1 receptor. While a tension of 10–15 mN/m may seem large experimentally, on the order of lytic tension for a typical membrane, simulations are limited by finite size effects that suppress long-range fluctuations in the small simulated membrane patches (see Marsh for a detailed discussion[76]). As a point of reference, reported lytic tensions in MD simulations of atomistic membranes are on the order of 40–45 mN/m.[47,48] We now test the ability of tension to induce activation starting from the inactive state of the AT1 receptor simulated in SOPC membranes. We applied increasing membrane tensions ranging from 5 to 20 mN/m in increments of 5 mN/m. In general, tension favors the outward movement of TM6 as can be seen by the increasing values of the TM1–TM6 distances in Figure 6a and Figure S7, although the extent of the movement and stability varies greatly between tensions and replicas. The TM1–TM6 distance is observed to reach its highest values of 26–29 Å for the moderate 5 and 10 mN/m tensions in the first set of replicas (Figure 6a), while it reaches values of up to 27 Å in the second 15 mN/m replica (Figure S7a). In many cases, the TM1–TM6 distances are observed to return to the inactive state value despite initially increasing.

Similarly to TM1–TM6, the TM3–TM6 distances increase to intermediate values at different times during the 5 μs simulations under tension, although often returning to inactive values later on as seen in Figure 6b and Figure S7b. While

https://doi.org/10.1021/acs.jpcb.4c03325
J. Phys. Chem. B 2024, 128, 9470–9481

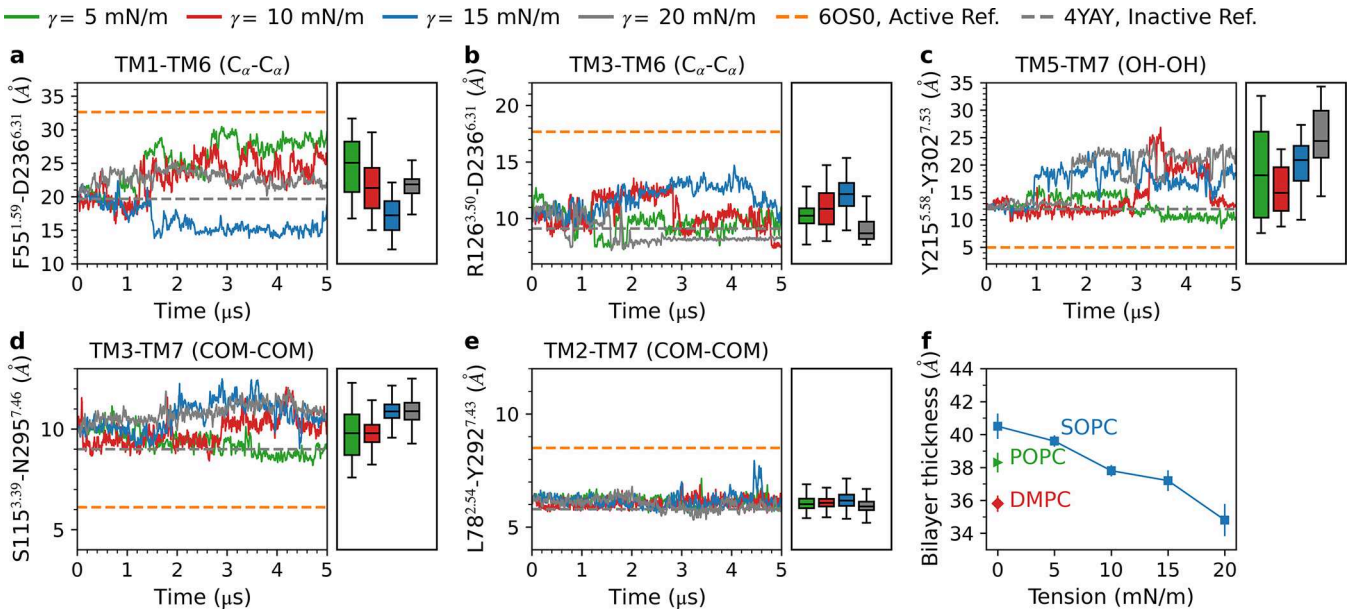

Figure 6. Driving activation of the AT1 receptor by membrane tension starting from the inactive state. Time evolution of apo-AT1 receptor simulations embedded in an SOPC membrane with varying membrane tensions (5−20 mN/m) for the first set of replicas. Large-scale conformational changes describing the inward/outward movement of TM6 are depicted by the TM1−TM6 (a) and TM3−TM6 (b) distances, while reorientation of local microswitches are described by the Y215−Y302 (NPxxY motif) (c), S115−N295 (d), and L78−Y292 (e) distances. Rectangular boxes on the right of each panel show box and whisker plots including median, quartiles, and extrema of the combined data from the two replicas of each system over the last 500 ns. Dashed gray and orange lines show values from crystal structures of the inactive receptor bound to a selective antagonist (4YAY) and active receptor bound to AngII (6OS0), respectively. (f) Average bilayer thickness computed from the peak-to-peak distance of the bilayer mass density over the last 500 ns. Error bars show the standard deviation from the mean. Membrane tension bolsters the larger movement of the TM helices (a, b) from the inactive state but does not appear to induce favorable changes in the other microswitches (c−e).

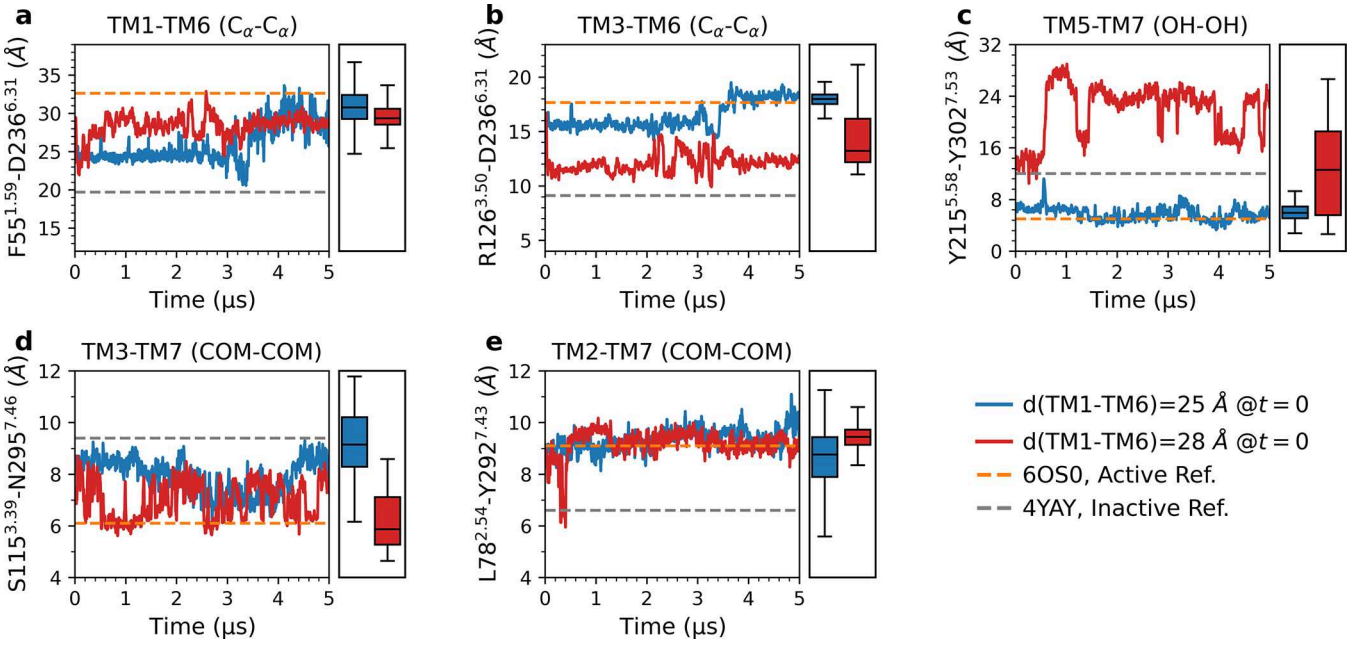

Figure 7. Testing the stability of intermediate states of the AT1 receptor by a membrane tension of 10 mN/m. Large-scale conformational changes describing the inward/outward movement of TM6 are depicted by the TM1−TM6 (a) and TM3−TM6 (b) distances, while reorientation of local microswitches are described by the Y215−Y302 (NPxxY motif) (c), S115−N295 (d), and L78−Y292 (e) distances using box and whisker plots (including median, quartiles, and extrema of the combined data from the two replicas of each system analyzed over the last 500 ns). Dashed gray and orange lines show values from crystal structures of the inactive receptor bound to a selective antagonist (4YAY) and active receptor bound to AngII (6OS0), respectively. Membrane tension is able to promote movement of the larger TM helical rearrangements and smaller microswitches toward the active configuration in many cases.

https://doi.org/10.1021/acs.jpcb.4c03325
J. Phys. Chem. B 2024, 128, 9470−9481

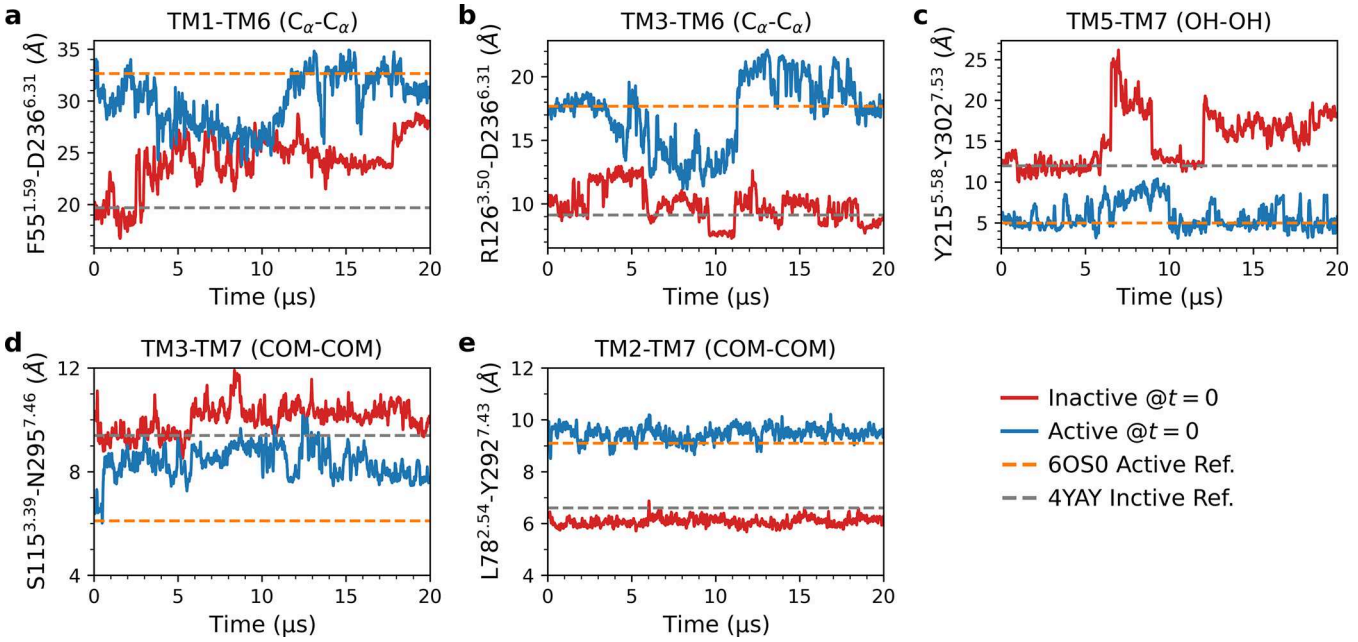

Figure 8. Long time scale dynamics of the AT1 receptor under tension (10 mN/m). Evolution of receptor simulations embedded in SOPC starting from active (blue lines, data from Poudel et al.[49]) vs inactive (red lines) configurations. Large-scale conformational changes describing the inward/outward movement of TM6 are depicted by the TM1−TM6 (a) and TM3−TM6 (b) distances, while reorientation of local microswitches are described by the Y215−Y302 (NPxxY motif) (c), S115−N295 (d), and L78−Y292 (e) distances. Dashed gray and orange lines show values from crystal structures of the inactive receptor bound to a selective antagonist (4YAY) and active receptor bound to AngII (6OS0) respectively. The receptor in an active-like state under tension undergoes long time-scale fluctuations (over several μs) and samples intermediate conformations. Similarly to the shorter simulations in Figure 6, running for longer time under tension from the inactive state mostly appears to favor the TM1−TM6 movement toward the active state.

tension appears to favor movement of the TM helices from the inactive to an active-like state, the local microswitches do not appear to similarly favor transition to active-like conformations during the time scale of the simulations (Figure 6c−e). As observed in the second replica of the DMPC system, the TM5−TM7 distance of the systems under tension increases beyond the inactive state value, which is due to increased tilt of TM5 due to hydrophobic mismatch as the bilayer thickness decreases. As membrane tension decreases the bilayer thickness due to incompressibility (Figure 6f), one cannot decouple the effects caused by the lateral forces and torques induced by membrane stretch from the hydrophobic mismatch, which likely plays a role in the ability of the TM helices to move past one another during activation/inactivation.

Another important factor to consider is the rate at which the membrane tension is established. In a typical membrane MD simulation, the membrane tension and corresponding area expansion will equilibrate in as little as 10−20 ns, which is likely much faster than what would be observed experimentally. Therefore, we tested the effect of gradually increasing the tension using two different approaches. First, we slowly ramped-up the tension in increments of 1 mN/m every 1 μs up to a final value of 10 mN/m (total simulation time of 10 μs) as shown in Figure S8. However, this showed no significant improvement compared to directly applying a constant tension of 10 mN/m from the beginning. Similarly, we extended the simulation time of the 5 mN/m simulation system to 10 μs followed by an increase to 10 mN/m for an additional 5 μs (Figure S9). In that simulation TM1−TM6 spends a considerable amount of time (~10 μs) in a high intermediate value near 26−30 Å, but returns to the inactive state value at the end of the 15 μs run (Figure S9). Both slow tension ramp-up strategies do not appear to favor a return to active values in the microswitches. However, the TM5−TM7 and TM3−TM7 distances sometimes extended beyond the inactive state values, because the larger hydrophobic mismatch induces a higher tilt angle of TM5 and TM7 with respect to the membrane normal, which may increase their separation distance.

In addition to starting from the inactive AT1 receptor under tension, we also tested the effect of moderate tension (10 mN/m) on the receptor in an SOPC membrane starting from intermediate states as shown in Figure 7 and Figure S10. These two intermediate configurations, where the TM1−TM6 distance is midway between fully active and inactive values, were chosen from a long simulation in the absence of tension from our previous work[49] (see Methods). The time traces for these simulations show that tension can drive the transition of TM1−TM6 and TM3−TM6 distances toward active-like states, although there are many fluctuations between active-like and intermediate values (see Figure 7a,b and Figure S10a,b). The individual microswitches also show high fluctuations which sometimes result in transitioning to the active-like or inactive state values depending on the residue pair and/or the simulation replica (see Figure 7c−e and Figure S10c−e).

Thus far, we have run extended simulations up to 5 μs for all of the different systems of interest with multiple replicas in most cases. However, it is clear from the observed dynamics that some of the transitions of the AT1 receptor occur over significantly longer time scales. We have further investigated the effect of 10 mN/m tension on the AT1 receptor in an SOPC membrane beginning from the inactive conformation, similarly to Figure 6, over a 4× longer simulation of 20 μs as

https://doi.org/10.1021/acs.jpcb.4c03325
J. Phys. Chem. B 2024, 128, 9470−9481

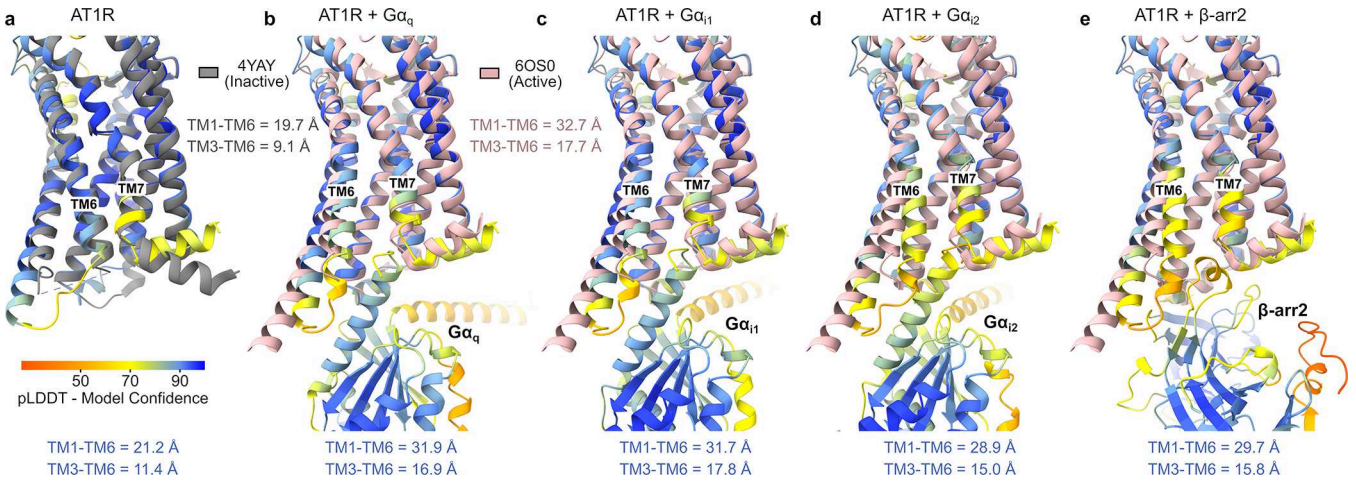

Figure 9. AlphaFold 2 predictions of the AT1 receptor in its apo state (a) and bound to four different effectors: (b) Gα_q, (c) Gα_{i1}, (d) Gα_{i2}, and (e) β-arr2. AF2 predictions are colored based on the pLDDT model confidence score (see Methods). Structures of the AT1 receptor in inactive (PDBID: 4YAY, gray) and active (PDBID: 6OS0, light pink) are shown for reference. Values of the TM1−TM6 and TM3−TM6 distances are shown next to the two reference experimental structures and below each of the AF2 models.

shown in Figure 8. Note that this is a different independent run and not just a continuation of the shorter simulation from that of the earlier figure. For comparison, we also include the data from our previous work[49] where the receptor in SOPC was simulated under the same tension of 10 mN/m starting from the active conformation. Over the long 20 μs simulation, we observe that tension favors the outward movement of TM1−TM6 from the inactive state, and this conformational change is continuously sustained (Figure 8a). When simulated from the inactive state under tension, the TM1−TM6 distance does not reach the fully activated value, but it does approach active-like states (~26−29 Å) which are also explored by the simulation started from the active state under tension. These active-like conformations are long-lived, as the systems in both cases remain near these values for many microseconds (5−10 μs). For the TM3−TM6 distance, we see that intermediate values are favored during the first 5 μs of the simulation starting from the inactive state and similar distances are explored by the receptor starting from the active state (Figure 8b). However, at later stages (>5 μs) in the simulation starting from the inactive state, the TM3−TM6 distance returns to inactive state values (Figure 8b). While the Y215−Y302 and L78−Y292 microswitches (Figure 8c,e) appear to be stable in the active configuration during the 20 μs simulation, tension alone does not appear to induce conformational switching of those residues from the inactive to the active state at these time scales.

Comparison with AlphaFold Predictions. While our simulation results thus far provide valuable insights into the effects of membrane thickness and tension on the stability and dynamics of the apo-AT1 receptor, it remains unclear how membrane-mediated stimuli will affect interaction with the different effector partners that include Gα_q, Gα_i, and β-arr2.[15,27] For example, the AT1 receptor directly binds Gα_q when activated by its natural agonist, AngII, while activation by biased agonists such as TRV023 promotes direct interaction with β-arr2.[25,77] Stretch-induced activation was originally proposed to occur through a direct interaction between the AT1 receptor and β-arr2 as osmotic stretch was shown to allosterically stabilize β-arrestin-biased conformations in cells expressing AT1R fused to β-arr2.[26] However, more recent studies indicate that binding of Gα_i is necessary for the recruitment of β-arr2.[15,27] It is important to note that in such an AT1R:Gα_i:β-arr2 complex, β-arr2 would primarily interact with Gα_i as the G-protein would occupy the receptor's canonical binding site.[27,78]

We can frame our simulation results within the context of these activation pathways through the use of AlphaFold 2 (AF2) multimeric structural predictions, as shown in Figure 9. While AF2 does not consider the surrounding membrane in its machine learning algorithm, it has been shown to successfully predict the structure of membrane proteins.[79] Furthermore, AF2 has been shown to accurately sample alternate conformational states of GPCRs.[80] In the absence of any ligand and/or binding partner, AF2 predicts that the apo-AT1 receptor will adopt an inactive configuration (Figure 9a) that closely resembles the structure of the receptor bound to the antagonist ZD7155 (PDBID: 4YAY). The model has a high degree of confidence, as measured by the pLDDT scores (see Methods), for the majority of the TM regions of the protein. The TM1−TM6 and TM3−TM6 distances for that AF2 model are also within 1−2 Å compared with the inactive state values (Figure 9a). AF2 predicts active-like configurations for the AT1 receptor when bound to Gα_q (Figure 9b) and Gα_{i1} (Figure 9c) showing a similar outward movement of TM6 compared to the active structure of the receptor with the AngII agonist (PDBID: 6OS0). The TM1−TM6 and TM3−TM6 distances for these two AF2 models are within 1 Å of the values observed in the active structure. However, the AF2 predicted models for the receptor interacting with Gα_{i2} (Figure 9d) and β-arr2 (Figure 9e) position TM6 more inwardly, while TM7 moves slightly outward. This repositioning of TM6 results in lower TM1−TM6 (~29−30 Å) and TM3−TM6 (~15−16 Å) distances, which are in the range of values observed in our simulations of active-like states in the SOPC membranes under tension. The intracellular portions of TM6 and TM7 in the Gα_{i2} and β-arr2 AF2 predictions show lower model confidence (~50−80 pLDDT) suggesting that the structure near this region may be more variable. While there are currently no available structures of the AT1 receptor interacting with G-proteins and/or β-arrestins, the presented AF2 models are in good agreement with experimentally obtained structures of β-

https://doi.org/10.1021/acs.jpcb.4c03325
J. Phys. Chem. B 2024, 128, 9470−9481

arr2 interacting with rhodopsin,[81] as well as Mas-related GPCR member X2 interacting with $G\alpha_q$ and $G\alpha_{i1}$[82] as shown in Figure S11. Together with our extensive simulation results, the AF2 predictions support the hypothesis that membrane tension may stabilize active-like states in the AT1 receptor that could bind certain effector partners such as β-arr2 or $G\alpha_i$.

CONCLUSIONS

We have presented a comprehensive computational study exploring the structure and dynamics of activation and inactivation by membrane thickness and far-field tension in the AT1 receptor through extensive multi-microsecond MD simulations (>175 μs total simulation time) and AlphaFold 2 multimeric predictions. Our results show that accessible configurational states of the receptor can be strongly modulated by the initial protein conformation (active or inactive) in addition to membrane conditions (different acyl-length and/or tension).

The large-scale conformational changes such as the outward motion of TM6, as measured by the TM1−TM6 and TM3−TM6 distances, are favorable in the large thickness SOPC membrane, where this helix is able to interchange between active-like, intermediate, and inactive positions over the course of several microseconds. In contrast to this, the TM6 motion was limited in the medium chain-length POPC and short DMPC membranes, where the helix remained near its initial position (active or inactive). Surprisingly, the local micro-switches do not show reversible behavior within the time scales explored in our study. These microswitches either remained in active-like orientations or transitioned to inactive configurations but rarely returned to active values once inactivated. Analysis of the membrane thickness in the vicinity of the AT1 receptor indicates that hydrophobic mismatch plays an important role in the ability of TM6 to move outward and inward during activation/inactivation. The thinner DMPC and POPC membranes pose a higher barrier for the movement of TM6 as these membranes require a larger local deformation compared to SOPC (Figure 5).

We have extensively tested the effect of membrane tension on both the stability of the active state of the AT1 receptor and the ability of tension to induce activation from an inactive configuration. Low or moderate tensions (5−10 mN/m) on the SOPC membrane favor the outward motion of TM6 to intermediate positions when simulated from a fully inactive state. Moderate membrane tension can also "pull" TM6 to an active-like position when starting from intermediate configurations. However, tension was not effective in promoting changes in the microswitches from inactive to active-like states during the time scales simulated. This is consistent with the observed behavior in the tensionless DMPC and POPC membranes which have a lower thickness compared to SOPC (Figure 3). Our simulation results suggest that membrane tension can induce and/or stabilize conformational changes, mainly the outward movement of TM6, in the AT1 receptor that could accommodate interactions with effectors such as β-arr2 or $G\alpha_{i2}$ but not $G\alpha_q$. This hypothesis is supported by the AF2 models presented above and is consistent with the previous experimental observations of tension-mediated interactions between the apo-AT1 receptor and β-arr2, which may occur through direct binding[26] or indirectly through $G\alpha_i$.[15]

ASSOCIATED CONTENT

Data Availability Statement

All data and python scripts used to generate the plots included in the manuscript are available in the following GitHub repository: https://github.com/Bharat-github6/JPCB_Structural_rearrangement_of_AT1R . This repository also contains PDB structures of the active and inactive structures of the AT1 receptor, simulation input files for GROMACS and Anton 2, and AlphaFold 2 predictions.

Supporting Information

The Supporting Information is available free of charge at https://pubs.acs.org/doi/10.1021/acs.jpcb.4c03325.

Time behavior of additional simulation replicas as well as comparison of AF2 predicted models with experimentally obtained structures (PDF)

AUTHOR INFORMATION

Corresponding Author

Juan M. Vanegas − *Department of Biochemistry and Biophysics, Oregon State University, Corvallis, Oregon 97331, United States;* orcid.org/0000-0003-1381-1649; Email: vanegasj@oregonstate.edu

Author

Bharat Poudel − *Department of Biochemistry and Biophysics, Oregon State University, Corvallis, Oregon 97331, United States*

Complete contact information is available at: https://pubs.acs.org/10.1021/acs.jpcb.4c03325

Notes

The authors declare no competing financial interest.

ACKNOWLEDGMENTS

JMV and BP acknowledge the support of the National Science Foundation through Grant No. CHE-1944892/2326678. Anton 2 computer time was provided by the Pittsburgh Supercomputing Center (PSC) through Grant R01GM116961 from the National Institutes of Health. The Anton 2 machine at PSC was generously made available by D. E. Shaw Research.

REFERENCES

(1) Sukharev, S.; Sachs, F. Molecular force transduction by ion channels: diversity and unifying principles. *J. Cell Sci.* **2012**, *125*, 3075−3083.

(2) Martinac, B.; Kung, C. The force-from-lipid principle and its origin, a 'what is true for *E. coli* is true for the elephant' refrain. *J. Neurogenet.* **2022**, *36*, 44−54.

(3) Kefauver, J. M.; Ward, A. B.; Patapoutian, A. Discoveries in structure and physiology of mechanically activated ion channels. *Nature* **2020**, *587*, 567−576.

(4) Booth, I. R.; Blount, P. The MscS and MscL families of mechanosensitive channels act as microbial emergency release valves. *J. Bacteriol.* **2012**, *194*, 4802−4809.

(5) Haswell, E. S.; Phillips, R.; Rees, D. C. Mechanosensitive channels: What can they do and how do they do it? *Structure* **2011**, *19*, 1356−1369.

(6) Brohawn, S. G.; del Mármol, J.; MacKinnon, R. Crystal structure of the human K2P TRAAK, a lipid-and mechano-sensitive K+ ion channel. *Science* **2012**, *335*, 436−441.

(7) Brohawn, S. G.; Su, Z.; MacKinnon, R. Mechanosensitivity is mediated directly by the lipid membrane in TRAAK and TREK1 K+ channels. *P. Natl. Acad. Sci. USA* **2014**, *111*, 3614−3619.

(8) Brohawn, S. G. How ion channels sense mechanical force: Insights from mechanosensitive K2P channels TRAAK, TREK1, and TREK2. *Ann. N.Y. Acad. Sci.* **2015**, *1352*, 20−32.
(9) Syeda, R.; Florendo, M. N.; Cox, C. D.; Kefauver, J. M.; Santos, J. S.; Martinac, B.; Patapoutian, A. Piezo1 channels are inherently mechanosensitive. *Cell Rep* **2016**, *17*, 1739−1746.
(10) Ranade, S. S.; Qiu, Z.; Woo, S.-H.; Hur, S. S.; Murthy, S. E.; Cahalan, S. M.; Xu, J.; Mathur, J.; Bandell, M.; Coste, B.; et al. Piezo1, a mechanically activated ion channel, is required for vascular development in mice. *P. Natl. Acad. Sci. USA* **2014**, *111*, 10347−10352.
(11) Ranade, S. S.; Woo, S.-H.; Dubin, A. E.; Moshourab, R. A.; Wetzel, C.; Petrus, M.; Mathur, J.; Bègay, V.; Coste, B.; Mainquist, J.; et al. Piezo2 is the major transducer of mechanical forces for touch sensation in mice. *Nature* **2014**, *516*, 121−125.
(12) Wilde, C.; Mitgau, J.; Suchý, T.; Schöneberg, T.; Liebscher, I. Translating the force—mechano-sensing GPCRs. *Am. J. Physiol.-Cell Ph.* **2022**, *322*, C1047−C1060.
(13) Zou, Y.; Akazawa, H.; Qin, Y.; Sano, M.; Takano, H.; Minamino, T.; Makita, N.; Iwanaga, K.; Zhu, W.; Kudoh, S.; et al. Mechanical stress activates angiotensin II type 1 receptor without the involvement of angiotensin II. *Nat. Cell Biol.* **2004**, *6*, 499−506.
(14) Tang, W.; Strachan, R. T.; Lefkowitz, R. J.; Rockman, H. A. Allosteric modulation of β-arrestin-biased angiotensin II Type 1 receptor signalling by membrane strecth. *J. Biol. Chem.* **2014**, *289*, 28271−28283.
(15) Wang, J.; Hanada, K.; Gareri, C.; Rockman, H. R. Mechano-sensation of the angiotension II type 1 receptor induces β-arrestin-biased signalling through Gαi coupling. *J. Cell Biochem.* **2018**, *119*, 3586−3597.
(16) Storch, U.; Schnitzler, M. M.; Gudermann, T. G. protein-mediated stretch reception. *Am. J. Physiol-Heart C.* **2012**, *302*, H1241−H1249.
(17) Jung, B.; Obinata, H.; Galvani, S.; Mendelson, K.; Ding, B.-s.; Skoura, A.; Kinzel, B.; Brinkmann, V.; Rafii, S.; Evans, T.; Hla, T. Flow-Regulated Endothelial S1P Receptor-1 Signaling Sustains Vascular Development. *Developmental Cell* **2012**, *23*, 600−610.
(18) Darby, W. G.; Potocnik, S.; Ramachandran, R.; Hollenberg, M. D.; Woodman, O. L.; McIntyre, P. Shear stress sensitizes TRPV4 in endothelium-dependent vasodilatation. *Pharmacol. Res.* **2018**, *133*, 152−159.
(19) Makino, A.; Prossnitz, E. R.; Bűnemann, M.; Wang, J. M.; Yao, W.; Schmid-schőnbein, G. W. G Protein-coupled receptors serve as mechanosensors for fluid shear stress in neutrophils. *Am. J. Physiol. Cell Physiol.* **2006**, *290*, C1633−C1639.
(20) Chachisvilis, M.; Zhang, Y.-L.; Frangos, J. A. G protein-coupled receptors sense fluid shear stress in endothelial cells. *Proc. Nat. Acad. Sci. USA* **2006**, *103*, 15463−15468.
(21) Abdul-Majeed, S.; Nauli, S. M. Dopamine receptor type 5 in primary cilia has dual chemo-and mechano-sensory roles. *Hypertension* **2011**, *58*, 325−331.
(22) Ainscough, J. F.; Drinkhill, M. J.; Sedo, A.; Turner, N. A.; Brooke, D. A.; Balmforth, A. J.; Ball, S. G. Angiotensin II type-1 receptor activation in the adult heart causes blood pressure-independent hypertrophy and cardiac dysfunction. *Cardiovasc. Res.* **2009**, *81*, 592−600.
(23) Manrique, C.; Lastra, G.; Gardner, M.; Sowers, J. R. The renin angiotensin aldosterone system in hypertension: Roles of insulin resistance and oxidative stress. *Med. Clin. North Am.* **2009**, *93*, 569−582.
(24) Ramchandran, R.; Takezako, T.; Saad, Y.; Stull, L.; Fink, B.; Yamada, H.; Dikalov, S.; Harrison, D. G.; Moravec, C.; Karnik, S. S. Angiotensinergic stimulation of vascular endothelium in mice causes hypotension, bradycardia, and attenuated angiotensin response. *Proc. Nat. Acad. Sci. USA* **2006**, *103*, 19087−19092.
(25) Dwivedi, H.; Baidya, M.; Shukla, A. K. GPCR signaling: The interplay of Gαi and β-arrestin. *Curr. Biol.* **2018**, *28*, R324−R327.
(26) Tang, W.; Strachan, R. T.; Lefkowitz, R. J.; Rockman, H. A. Allosteric modulation of β-arrestin-biased angiotensin II type 1 receptor signaling by membrane stretch. *J. Biol. Chem.* **2014**, *289*, 28271−28283.
(27) Smith, J. S.; Pack, T. F.; Inoue, A.; Lee, C.; Zheng, K.; Choi, I.; Eiger, D. S.; Warman, A.; Xiong, X.; Ma, Z.; et al. Noncanonical scaffolding of Gαi and β-arrestin by G protein−coupled receptors. *Science* **2021**, *371*, eaay1833.
(28) Andersen, O. S.; Koeppe, R. E. Bilayer thickness and membrane protein function: an energetic perspective. *Annu. Rev. Biophys. Biomol. Struct.* **2007**, *36*, 107−130.
(29) Levental, I.; Lyman, E. Regulation of membrane protein structure and function by their lipid nano-environment. *Nat. Rev. Mol. Cell Biol* **2023**, *24*, 107−122.
(30) Gahbauer, S.; Böckmann, R. A. Membrane-Mediated Oligomerization of G Protein Coupled Receptors and Its Implications for GPCR Function. *Front. Physiol.* **2016**, *7*, 494.
(31) Alemany, R.; Perona, J. S.; Sánchez-Dominguez, J. M.; Montero, E.; Cañizares, J.; Bressani, R.; Escribá, P. V.; Ruiz-Gutierrez, V. G protein-coupled receptor systems and their lipid environment in health disorders during aging. *BBA - Biomembranes* **2007**, *1768*, 964−975.
(32) Goddard, A. D.; Dijkman, P. M.; Adamson, R. J.; Watts, A. Lipid-dependent GPCR dimerization. *Methods Cell Biol.* **2013**, *117*, 341−357.
(33) Killian, J. A. Hydrophobic mismatch between proteins and lipids in membranes. *BBA Rev. Biomembr.* **1998**, *1376*, 401−416.
(34) Escribá, P. V.; Wedegaertner, P. B.; Goñi, F. M.; Vögler, O. Lipid−protein interactions in GPCR-associated signaling. *BBA - Biomembranes* **2007**, *1768*, 836−852.
(35) Dijkman, P. M.; Watts, A. Lipid modulation of early G protein-coupled receptor signalling events. *BBA - Biomembranes* **2015**, *1848*, 2889−2897.
(36) Kockelkoren, G.; Lauritsen, L.; Shuttle, C. G.; Kazepidou, E.; Vonkova, I.; Zhang, Y.; Breuer, A.; Kennard, C.; Brunetti, R. M.; D'Este, E.; et al. Molecular mechanism of GPCR spatial organization at the plasma membrane. *Nat. Chem. Biol.* **2024**, *20*, 142−150.
(37) Botelho, A. V.; Huber, T.; Sakmar, T. P.; Brown, M. F. Curvature and Hydrophobic Forces Drive Oligomerizatonion and Modulate Activity of Rhodopsin in Membranes. *Biophys. J.* **2006**, *91*, 4464−4477.
(38) Soubias, O.; Niu, S.-L.; Mitchell, D. C.; Gawrisch, K. Lipid-Rhodopsin Hydrophobic mismatch alters Rhodopsin Helical content. *J. Am. Chem. Soc.* **2008**, *130*, 12465−12471.
(39) Soubias, O.; Teague Jr, W. E.; Hines, K. G.; Gawrisch, K. Rhodopsin/Lipid Hydrophobic Matching-Rhodopsin Oligomerization and Function. *Biophys. J.* **2015**, *108*, 1125−1132.
(40) Damian, M.; Louet, M.; Gomes, A. A. S.; M'Kadmi, C.; Denoyelle, S.; Cantel, S.; Mary, S.; Fehrentz, J.-A.; Catoire, L. J.; Floquet, N.; et al. Allosteric modulation of ghrelin receptor signaling by lipids. *Nat. Commun.* **2021**, *12*, 3938.
(41) Lorent, J. H.; Levental, K. R.; Ganesan, L.; Rivera-Longsworth, G.; Sezgin, E.; Doktorova, M.; Lyman, E.; Levental, I. Plasma membranes are asymmetric in lipid unsaturation, packing and protein shape. *Nat. Chem. Biol.* **2020**, *16*, 644−652.
(42) Foley, S. L.; Varma, M.; Hossein, A.; Deserno, M. Elastic and thermodynamic consequences of lipid membrane asymmetry. *Emerg. Top. Life Sci.* **2023**, *7*, 95−110.
(43) Deserno, M. Biomembranes balance many types of leaflet asymmetries. *Curr. Opin. Struc Biol.* **2024**, *87*, 102832.
(44) Vanegas, J. M.; Torres-Sánchez, A.; Arroyo, M. Importance of force decomposition for local stress calculations in biomembrane molecular simulations. *J. Chem. Theory Comput.* **2014**, *10*, 691−702.
(45) Torres-Sánchez, A.; Vanegas, J. M.; Arroyo, M. Examining the mechanical equilibrium of microscopic stresses in molecular simulations. *Phys. Rev. Lett.* **2015**, *114*, 258102.
(46) Vanegas, J. M.; Arroyo, M. Force transduction and lipid binding in MscL: A continuum-molecular approach. *PLoS ONE* **2014**, *9*, No. e113947.
(47) Sharma, A.; Anishkin, A.; Sukharev, S.; Vanegas, J. M. Tight hydrophobic core and flexible helices yield MscL with a high tension

https://doi.org/10.1021/acs.jpcb.4c03325
J. Phys. Chem. B 2024, 128, 9470−9481

gating threshold and a membrane area mechanical strain buffer. *Front. Chem.* **2023**, *11*, 1159032.
(48) Rajeshwar T., R.; Anishkin, A.; Sukharev, S.; Vanegas, J. M. Mechanical Activation of MscL Revealed by a Locally Distributed Tension Molecular Dynamics Approach. *Biophys. J.* **2021**, *120*, 232−242.
(49) Poudel, B.; Rajeshwar T., R.; Vanegas, J. M. Membrane mediated mechanical stimuli produces distinct active-like states in the AT1 receptor. *Nat. Commun.* **2023**, *14*, 4690.
(50) Abraham, M. J.; Murtola, T.; Schulz, R.; Páll, S.; Smith, J. C.; Hess, B.; Lindahl, E. GROMACS: High performance molecular simulations through multi-level parallelism from laptops to supercomputers. *SoftwareX* **2015**, *1−2*, 19−25.
(51) Mackerell, A. D.; Bashford, D.; Bellott, M.; Dunbrack, R. L.; Evanseck, J. D.; Field, M. J.; Fischer, S.; Gao, J.; Guo, H.; Ha, S.; et al. All-atom empirical potential for molecular modeling and dynamics studies of proteins. *J. Phys. Chem. B* **1998**, *102*, 3586−3616.
(52) Best, R. B.; Zhu, X.; Shim, J.; Lopes, P. E. M.; Mittal, J.; Feig, M.; Mackerell, A. D., Jr. Optimization of the Additive CHARMM All-Atom Protein Force Field Targeting Improved Sampling of the Backbone ϕ, ψ and Side-Chain χ_1 and χ_2 Dihedral Angles. *J. Chem. Theory Comput.* **2012**, *8*, 3257−3273.
(53) Huang, J.; Rauscher, S.; Nawrocki, G.; Ran, T.; Feig, M.; de Groot, B. L.; Grubmüller, H.; Mackerell, A. D. CHARMM36m: an improved force field for folded and intrinsically disordered proteins. *Nat. Methods* **2017**, *14*, 71−73.
(54) Klauda, J. B.; Venable, R. M.; Freites, J. A.; O'Connor, J. W.; Tobias, D. J.; Mondragon-Ramirez, C.; Vorobyov, I.; Mackerell, A. D.; Pastor, R. W. Update of the CHARMM All-Atom Additive Force Field for Lipids: Validation on Six Lipid Types. *J. Phys. Chem. B* **2010**, *114*, 7830−7843.
(55) Pastor, R. W.; Mackerell, A. D. Development of the CHARMM Force Field for Lipids. *J. Phys. Chem. Lett.* **2011**, *2*, 1526−1532.
(56) Wingler, L. M.; McMahon, C.; Staus, D. P.; Lefkowitz, R. J.; Kruse, A. C. Distinctive Activation Mechanism for Angiotensin Receptor Revealed by a Synthetic Nanobody. *Cell* **2019**, *176*, 479−490.
(57) Suomivuori, C.-M.; Latorraca, N. R.; Wingler, L. M.; Eismann, S.; King, M. C.; Kleinhenz, A. L. W.; Skiba, M. A.; Staus, D. P.; Kruse, A. C.; Lefkowitz, R. J.; Dror, R. O. Molecular Mechanism of biased signalling in a prototypical G Protein-coupled receptor. *Science* **2020**, *367*, 881−887.
(58) Ballesteros, J. A.; Weinstein, H. In *Receptor Molecular Biology*; Sealfon, S. C., Ed.; Methods in Neurosciences; Academic Press, 1995; Vol. *25*, pp 366−428.
(59) Webb, B.; Sali, A. Comparative Protein Structure Modeling Using MODELLER. *Curr. Protoc. Bioinform* **2016**, *54*, 5.6.1−5.6.37.
(60) Shaw, D. E.; Grossman, J.; Bank, J. A.; Batson, B.; Butts, J. A.; Chao, J. C.; Deneroff, M. M.; Dror, R. O.; Even, A.; Fenton, C. H. et al. Anton 2: Raising the Bar for Performance and Programmability in a Special-Purpose Molecular Dynamics Supercomputer. *SC '14: Proceedings of the International Conference for High Performance Computing, Networking, Storage and Analysis*. 2014; pp 41−53.
(61) Lippert, R. A.; Predescu, C.; Ierardi, D. J.; Mackenzie, K. M.; Eastwood, M. P.; Dror, R. O.; Shaw, D. E. Accurate and efficient integration for molecular dynamics simulations at constant temperature and pressure. *J. Chem. Phys.* **2013**, *139*, 164106.
(62) Shan, Y.; Klepeis, J. L.; Eastwood, M. P.; Dror, R. O.; Shaw, D. E. Gaussian split Ewald: A fast Ewald mesh method for molecular simulation. *J. Chem. Phys.* **2005**, *122*, 054101.
(63) Martyna, G. J.; Tobias, D. J.; Klein, M. L. Constant pressure molecular dynamics algorithms. *J. Chem. Phys.* **1994**, *101*, 4177−4189.
(64) Wingler, L. M.; Skiba, M. A.; McMahon, C.; Staus, D. P.; Kleinhenz, A. L. W.; Suomivuori, C.-M.; Latorraca, N. R.; Dror, R. O.; Lefkowitz, R. J.; Kruse, A. C. Angiotensin and biased analogs induce structurally distinct active conformations within a GPCR. *Science* **2020**, *367*, 888−892.
(65) Hunter, J. D. Matplotlib: A 2D graphics environment. *Comput. Sci. Eng.* **2007**, *9*, 90−95.
(66) Pettersen, E. F.; Goddard, T. D.; Huang, C. C.; Couch, G. S.; Greenblatt, D. M.; Meng, E. C.; Ferrin, T. E. UCSF Chimera—a visualization system for exploratory research and analysis. *J. Comput. Chem.* **2004**, *25*, 1605−1612.
(67) Goddard, T. D.; Huang, C. C.; Meng, E. C.; Pettersen, E. F.; Couch, G. S.; Morris, J. H.; Ferrin, T. E. UCSF ChimeraX: Meeting modern challenges in visualization and analysis. *Protein Sci.* **2018**, *27*, 14−25.
(68) Jumper, J.; Evans, R.; Pritzel, A.; Green, T.; Figurnov, M.; Ronneberger, O.; Tunyasuvunakool, K.; Bates, R.; Žídek, A.; Potapenko, A.; et al. Highly accurate protein structure prediction with AlphaFold. *Nature* **2021**, *596*, 583−589.
(69) Mirdita, M.; Schütze, K.; Moriwaki, Y.; Heo, L.; Ovchinnikov, S.; Steinegger, M. ColabFold: Making Protein folding accessible to all. *Nat. Methods* **2022**, *19*, 679−682.
(70) Mirdita, M.; von den Driesch, L.; Galiez, C.; Martin, M. J.; Söding, J.; Steinegger, M. Uniclust databases of clustered and deeply annotated protein sequences and alignments. *Nucleic Acids Res.* **2017**, *45*, D170−D176.
(71) Mirdita, M.; Steinegger, M.; Söding, J. MMseqs2 desktop and local web server app for fast, interactive sequence searches. *Bioinformatics* **2019**, *35*, 2856−2858.
(72) The UniProt Consortium. UniProt: the Universal Protein Knowledgebase in 2023. *Nucleic Acids Res.* **2023**, *51*, D523−D531.
(73) Smith, S. O. Deconstructing the transmembrane core of class A G protein−coupled receptors. *Trends Biochem. Sci.* **2021**, *46*, 1017−1029.
(74) Weis, W. I.; Kobilka, B. K. The Molecular Basis of G Protein-Coupled Receptor Activation. *Annu. Rev. Biochem.* **2018**, *87*, 897−919.
(75) Shao, Z.; Shen, Q.; Yao, B.; Mao, C.; Chen, L.-N.; Zhang, H.; Shen, D.-D.; Zhang, C.; Li, W.; Du, X.; et al. Identification and mechanism of G protein-biased ligands for chemokine receptor CCR1. *Nat. Chem. Biol.* **2022**, *18*, 264−271.
(76) Marsh, D. Renormalization of the tension and area expansion modulus in fluid membranes. *Biophys. J.* **1997**, *73*, 865−869.
(77) Turu, G.; Balla, A.; Hunyady, L. The role of β-arrestin proteins in organization of signalling and regulation of AT1 angiotensin receptor. *Front. Endocrinol.* **2019**, *10*, 519.
(78) Nguyen, A. H.; Thomsen, A. R. B.; Cahill, T. J.; Huang, R.; Huang, L.-Y.; Marcink, T.; Clarke, O. B.; Heissel, S.; Masoudi, A.; Ben-Hail, D.; et al. Structure of an endosomal signaling GPCR−G protein−β-arrestin megacomplex. *Nat Struct Mol Biol* **2019**, *26*, 1123−1131.
(79) Hegedűs, T.; Geisler, M.; Lukács, G. L.; Farkas, B. Ins and outs of AlphaFold2 transmembrane protein structure predictions. *Cell. Mol. Life Sci.* **2022**, *79*, 73.
(80) del Alamo, D.; Sala, D.; Mchaourab, H. S.; Meiler, J. Sampling alternative conformational states of transporters and receptors with AlphaFold2. *eLife* **2022**, *11*, No. e75751.
(81) Kang, Y.; Zhou, X. E.; Gao, X.; He, Y.; Liu, W.; Ishchenko, A.; Barty, A.; White, T. A.; Yefanov, O.; Han, G. W.; et al. Crystal structure of rhodopsin bound to arrestin by femtosecond X-ray laser. *Nature* **2015**, *523*, 561−567.
(82) Cao, C.; Kang, H. J.; Singh, I.; Chen, H.; Zhang, C.; Ye, W.; Hayes, B. W.; Liu, J.; Gumpper, R. H.; Bender, B. J.; et al. Structure, function and pharmacology of human itch GPCRs. *Nature* **2021**, *600*, 170−175.

https://doi.org/10.1021/acs.jpcb.4c03325
J. Phys. Chem. B 2024, 128, 9470−9481